MATERIALS CHEMISTRY FRONTIERS

RESEARCH ARTICLE

View Article Online
View Journal | View Issue



Cite this: *Mater. Chem. Front.*, 2022, **6**, 2796

# High-entropy-alloy nanoparticles synthesized by laser metallurgy using a multivariate MOF†

Wei Yan, ‡[ab] Haoqing Jiang,‡[cd] Wendi Yi,‡[d] Chengbin Zhao,[b] Yucong Xia,[b] Hengjiang Cong,[b] Lin Tang,*[ac] Gary J. Cheng,*[de] Jianhua He*[a] and Hexiang Deng*[abc]

Received 20th June 2022,
Accepted 8th August 2022

DOI: 10.1039/d2qm00588c

rsc.li/frontiers-materials



We report the synthesis of multivariate MOFs with combinations of metal ions, including $Mn^{2+}$, $Fe^{3+}$, $Co^{2+}$, $Ni^{2+}$, $Cu^{2+}$ and $Zn^{2+}$. The permanent porosity and the evenly distributed metal components make these porous crystals ideally suited for the synthesis of alloy nanoparticles. Using a laser, these MOFs are converted in air to alloy nanoparticles of binary (FeNi, FeCo), ternary (FeCoNi) and high-entropy-alloys with quinary (MnFeCoNiCu, MnFeCoNiZn) metals. One member, FeNi alloy nanoparticles with a narrow particle size distribution around 7 nm, shows a low overpotential of 282 mV at a current density of 10 mA $cm^{-2}$ in the oxygen evolution reaction (OER), better than those of the single metal counterparts. This demonstrates the possibility of using MOFs to produce alloy nanoparticles with multiple metal components by a laser.

Combining various metals at atomic scale to form metal alloys is an effective way to explore their optical, magnetic and catalytic properties.[1–3] The heterometals form a unique interface for the precise tuning of the Fermi energy, electron structure and work function beyond those of monometallic materials. This offers an opportunity to use alloys of natural abundant metals for the replacement of noble metals in industrial applications.[4,5] It remains challenging, however, to obtain alloys with an even distribution of metals at the atomic scale, when the number of metal types becomes large. This is due to the difference of metals in their electronegativity, size and preferred packing in a lattice. Making alloys into nanoscale might possibly address the compatibility issue at the atomic scale. Typically, materials are regarded as high-entropy-alloy nanoparticles (HEANPs) when the number of metal components goes beyond 5.[6–13] The formation of a high entropy compound usually involves a kinetically controlled process, with stringent requirement on the precursor and temperature.[14,15]

Metal–organic frameworks (MOFs) are porous crystals constructed by alternating arrangement of metal clusters and organic linkers,[16,17] standing as ideal precursors with atomic precision of the metal distribution. The rich choices both in the metal clusters and the organic linkers leads to the emergence of multivariate metal–organic frameworks (MTV-MOFs), where different organic linkers and metals in the secondary building units (SBUs) can be introduced into the structure without altering the backbone.[18,19] The customized pore environment in MTV-MOFs leads to excellent performances in various applications.[20–22] As the precursor for the conversion to metal nanoparticles, the carbonaceous linkers adjacent to metal ions naturally produce a reductive environment for metallurgy.[23] Theoretically, it's straight forward to obtain alloy nanoparticles from MTV-MOFs with multiple metal components. In fact, there are very few works reported using the MTV-MOF strategy for the fabrication of alloy nanoparticles,[23–25] and the metal components have yet go beyond two types, due to the poor compatibility of various metal ions in the SBU of MTV-MOFs and/or the loss of permanent porosity. In this work, we show that a series of MTV-MOFs containing various metal ions can be applied as precursors for the production of alloy nanoparticles with up to 5 components. The corresponding alloy nanoparticles are generated by a recently developed strategy, laser metallurgy, where these MTV-MOFs are subjected to instant heating and cooling induced by a pulsed laser.[23–27] The $M_3O_{13}N_3$ SBUs with high connectivity of 9, and organic linker (4,4′-(pyridine-3,5-diyl)dibenzoic acid, PDA) with 3 connectivity sites are assembled into a series of isoreticular MOFs, CPM-70, with high stability and permanent porosity (Fig. 1A and B). We found that the trinucleate metal oxide clusters in CPM-70 exhibited excellent compatibility for various transition metals,

[a] *The Institute for Advanced Studies, Wuhan University, Wuhan 430072, China. E-mail: lintang@whu.edu.cn, hejianhua@whu.edu.cn, hdeng@whu.edu.cn*
[b] *College of Chemistry and Molecular Sciences, Wuhan University, Wuhan 430072, China*
[c] *Hubei Yangtze Memory Laboratories, Wuhan 430205, China*
[d] *The Institute of Technological Sciences, Wuhan University, Wuhan 430072, China*
[e] *School of Industrial Engineering, Purdue University, West Lafayette 47906, Indiana, USA. E-mail: gjcheng@purdue.edu*

† Electronic supplementary information (ESI) available. See DOI: https://doi.org/10.1039/d2qm00588c

‡ These authors contributed equally to this work.

 

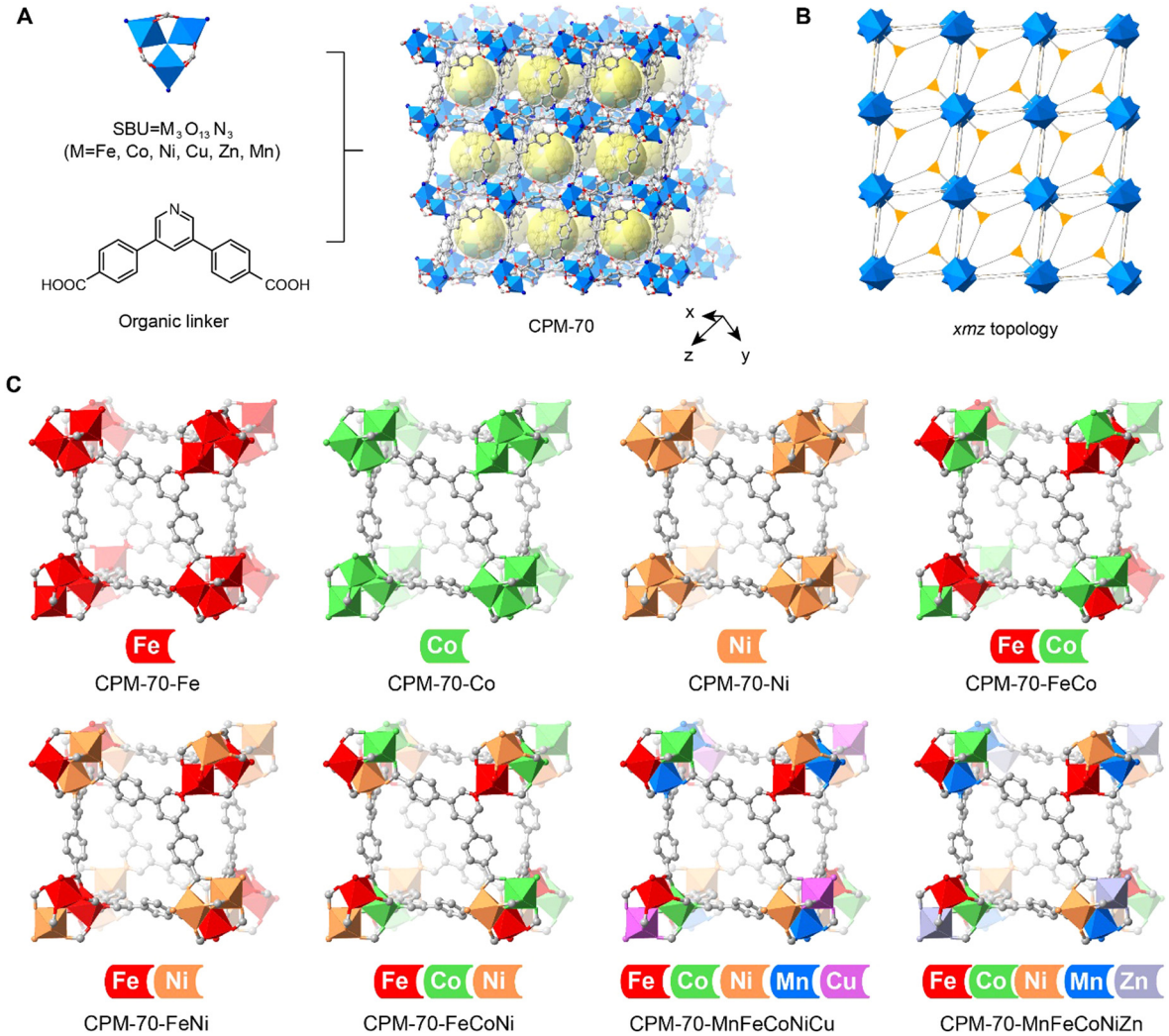


Fig. 1 (A) The construction of CPM-70 using a 9-connected (9-c) metal oxide cluster and 3-connected (3-c) organic linker. (B) The xmz topology of the CPM-70. (C) The incorporation of unary, binary, ternary and quinary metal ions in the isoreticular CPM-70 serial MOFs as precursors for the production of alloy nanoparticles by laser metallurgy.

such as $Mn^{2+}$, $Fe^{3+}$, $Co^{2+}$, $Ni^{2+}$, $Cu^{2+}$ and $Zn^{2+}$, leading to the successful fabrication of a series of MTV-MOFs containing unary, binary, ternary and quinary metals (Fig. 1C). When irradiated by a nanosecond pulsed laser, these MTV-MOF precursors are instantly converted to the corresponding metal nanoparticles, including high-entropy-alloy nanoparticles. The combination of the MTV-MOF strategy and the laser metallurgy method provides a new route for the synthesis of high-entropy-alloy nanoparticles in a fast and designable manner.

The synthesis of the isoreticular CPM-70 serial MOFs with various metal ions in the SBU was based on a reported solvothermal reaction with slight modifications.[28–31] The PDA ligand was synthesized in a two-step reaction with a yield of 85% (Fig. S1–S7, ESI†). The isoreticular CPM-70 with designated metal ions in the SBU was obtained by mixing of the metal ions in the mother solvent. CPM-70 with unary metals, CPM-70-Fe, CPM-70-Co and CPM-70-Ni, were cubic crystals with size around 200 μm after solvothermal reaction of the metal ions and organic linker in DMF with an incubation time of 24 h at 150 °C (Fig. S8, ESI†). Single crystal X-ray diffraction (SCXRD) analysis of these MOF crystals showed that they had isoreticular xmz topology, and slightly varied cell parameters (Tables S1–S3, ESI†). The MTV-MOFs, such as CPM-70-MnFeCoNiCu crystals also appeared in cubic shape; however, they preserved a smaller size of around 5 μm (Fig. 2G).

The homogeneous dispersion of metal ions within MTV-MOFs was confirmed by energy-dispersive spectroscopy (EDS) in scanning electron microscopy (SEM) and transmission electron microscopy (TEM) (Fig. 2A–G and Fig. S9, ESI†). When binary and ternary metal ions were introduced in the CPM-70, such as Fe/Co, Fe/Ni, and Fe/Co/Ni, they showed identical elemental signals with C and N signals from the linker, implying that these metals were in a well-mixed manner and evenly dispersed across the MOF crystals. When the species of the metal ions increased to 5, Mn/Fe/Co/Ni/Zn or Mn/Fe/Co/Ni/Cu, for instance, they still maintained identical signal distribution

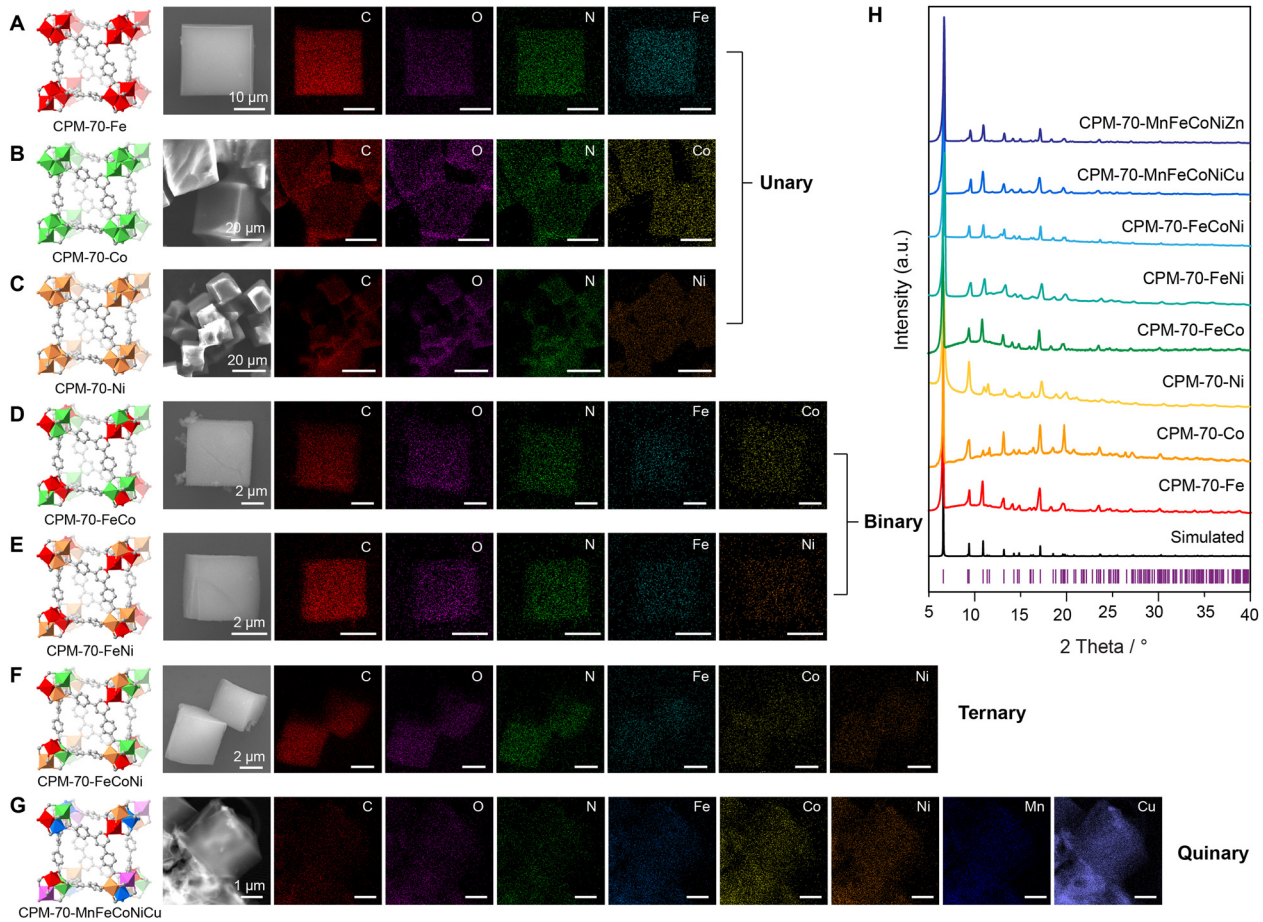


Fig. 2 The crystalline structure and corresponding elemental mappings of (A) CPM-70-Fe, (B) CPM-70-Co, (C) CPM-70-Ni, (D) CPM-70-FeCo, (E) CPM-70-FeNi, (F) CPM-70-FeCoNi, and (G) CPM-70-MnFeCoNiCu. (H) The PXRD patterns of the isoreticular CPM-70 serial MOF precursors containing various metal ions in the SBU.

with the C and N (Fig. 2G and Fig. S9, ESI†), suggesting that the trinucleate metal clusters had high compatibility with different metal ions. All the synthesized isoreticular MOFs exhibited identical powder X-ray diffraction (PXRD) patterns and matched well with the simulated one from the single crystal data (Fig. 2H), demonstrating their phase purities.

The permanent porosity of these MTV-MOFs was evaluated by nitrogen adsorption isotherms measured at 77 K. The guest molecules in the pores of these MOFs could be successfully removed by solvent exchange and supercritical $CO_2$ activation without altering the crystallinity. This was proved by the identical PXRD patterns before and after activation (Fig. S10–S17, ESI†). High Brunauer–Emmett–Teller (BET) surface areas of 1930, 920, 1050, 1380, 1540, 1600, 1520, and 1380 $m^2\ g^{-1}$ were observed in CPM-70-Fe, CPM-70-Co, CPM-70-Ni, CPM-70-FeCo, CPM-70-FeNi, CPM-70-FeCoNi, CPM-70-MnFeCoNiCu, and CPM-70-MnFeCoNiZn, respectively (Fig. S18–S25, ESI†). The high porosity in the MTV-MOFs benefits their conversion to alloy nanoparticles by laser metallurgy. These MTV-MOFs with high connectivity also exhibited high chemical stability, which could be revealed by the well-maintained PXRD patterns before and after immersing these MOF crystals in $H_2O$, HCl (PH = 4) or NaOH (PH = 9) for 6 h (Fig. S26–S28, ESI†). Thermo-gravimetric analysis (TGA) uncovered that these MTV-MOFs also had high thermal stability and decomposed at around 400 °C in air (Fig. S29–S36, ESI†). The successful incorporation of various metal ions in the activated MOF precursor was analyzed by inductively coupled plasma atomic emission spectroscopy (ICP-AES) (Table S4, ESI†). When a feeding ratio of Mn/Fe/Co/Ni/Zn = 1 : 1 : 1 : 1 : 1 was applied in the mother solvent of the MOF, the obtained MOF exhibited a corresponding ratio of 1 : 1.32 : 1.54 : 1.55 : 1.49.

The even dispersion of different metal ions in the MTV-MOF provides an ideal precursor for the production of uniform nanoalloys by ultrafast laser nanometallurgy.[24,32] The operation of laser nanometallurgy for the conversion of the MTV-MOF to the corresponding nanoalloys was achieved by irradiation of the powdery MOF precursor sandwiched between two glass slides. The nanosecond pulsed laser was operated at a wavelength of 1064 nm, frequency of 20 kHz, pulse energy of 30 mJ, beam size of 200 μm, and scribing speed of 75 mm $s^{-1}$. Once laser scribed, the pristine MOF layer instantly turned black, indicating the successful conversion of the MOF precursor to a carbonaceous support. A previous study revealed that the laser nanometallurgy method could convert the transition metal ions

 

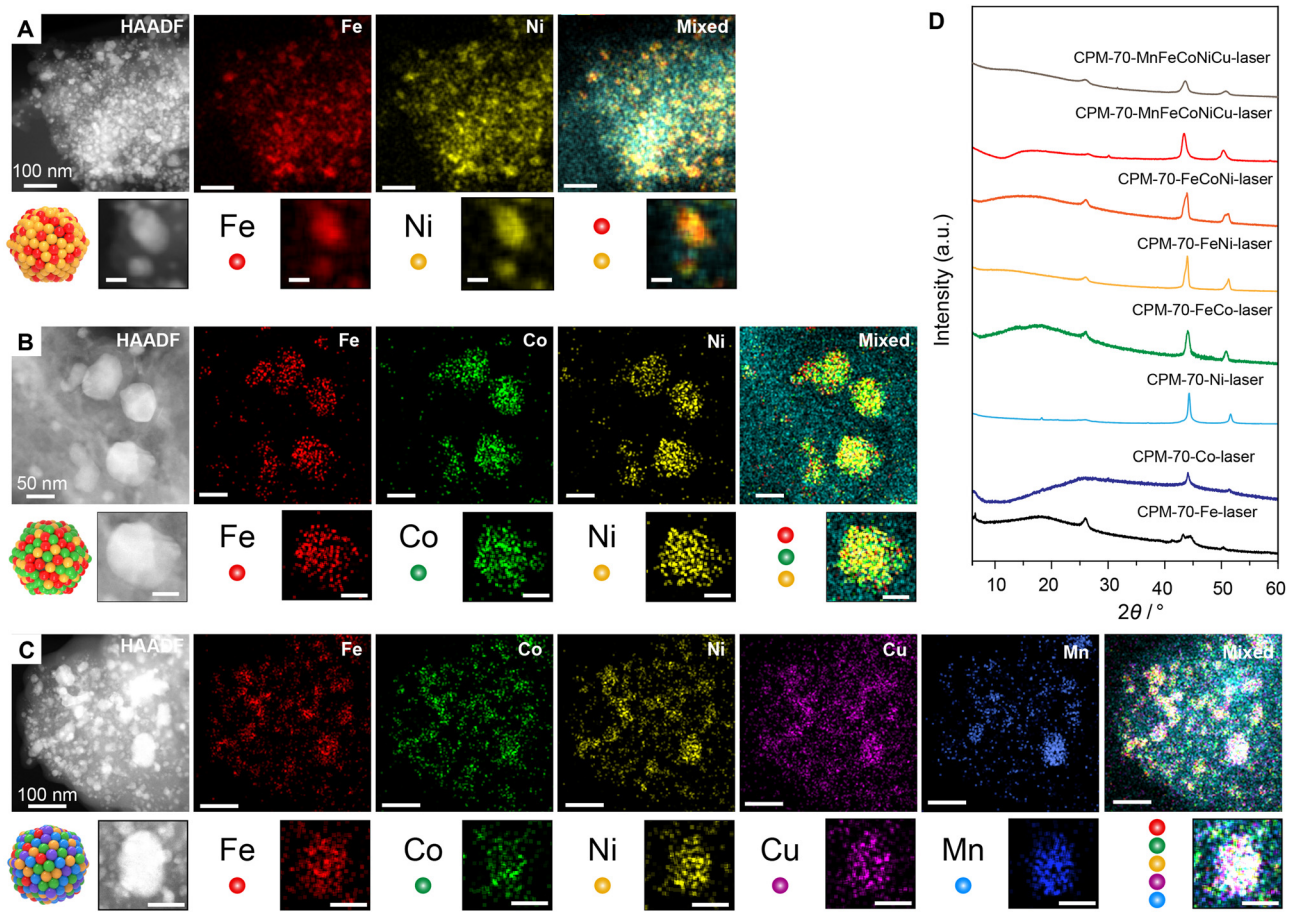


Fig. 3 The TEM images and the elemental mappings of (A) FeNi, (B) FeCoNi, and (C) FeCoNiCuMn nanoalloys from laser metallurgy of the corresponding MOF precursors and the corresponding alloy nanoparticle models to illustrate the distribution of elements in the nanoparticles. (D) The PXRD patterns of the nanoalloys converted from the corresponding MOF precursors. The scale bar is 5 nm, 20 nm, and 50 nm in the magnified TEM image and elemental mappings in (A–C), respectively.

in the MOF to the corresponding MNPs because of the localized reductive atmosphere formed around the laser irradiated spots.[24] In the case of MTV-MOF with various transition metal ions in the SBU, the instant heating and cooling should lead to the formation of nanoalloys without segregation into metallic phases.[7] The laser processed product, denoted as CPM-70-M-laser (M represents the metal ions in the SBU), was collected and characterized. The SEM images showed that all the CPM-70-M-laser samples exhibited an amorphous and porous structure with nanoparticles embedded (Fig. S37–S44, ESI†).

To demonstrate the well-mixed nature of different metals in the nanoalloys derived from these MTV-MOFs, elemental mappings were collected from energy dispersive spectroscopy (EDS) (Fig. 3A–C). The elemental mappings of the binary FeNi nanoalloy also confirmed the uniform distribution of Fe and Ni across the nanoparticles (Fig. 3A). The ternary FeCoNi nanoalloys also exhibited well mixed nature of the three elements across the nanoparticles (Fig. 3B). When the metal elements increased to five, in CPM-70-MnFeCoNiZn-laser for example, all the five metals showed similar distribution in each nanoparticle (Fig. 3C), suggesting the successful formation of HEANPs.[7] The successful conversion of the MTV-MOF precursor to the nanoalloys was also proved by the PXRD patterns (Fig. 3D). No obvious peaks assigned to the pristine MOF were observed, suggesting their complete conversions. The broad peak at $2\theta = 26^\circ$ was ascribed the 001 facet of graphite and the two peaks located around $2\theta = 45^\circ$ and $52^\circ$ were assigning to the facets of 110 and 200 of nanoalloys in fcc. No obvious peaks from the unary metals were observed in the product from MTV-MOF (Fig. S45, ESI†), demonstrating the well-mixed nature of the metals in the nanoparticles. Even encapsulated with 5 metals, the PXRD pattern of the CPM-70-MnFeCoNiCu-laser only preserved peaks assigned to fcc alloys, revealing the capability to produce HEANPs from MTV-MOF by laser metallurgy.

We found that uniform binary FeNi nanoalloys with an averaged size of 7 nm could be successfully synthesized by laser metallurgy from the CPM-70-FeNi precursor (Fig. 4A and B). The high-resolution TEM images revealed the lattice distance of 0.21 nm (Fig. 3A), consistent with the 111 lattice plane of the FeNi nanoalloy. The selected area electron diffraction (SAED) pattern of the FeNi nanoalloys also revealed their fcc phase. Notably, larger particles of FeC and Ni were observed from the corresponding unary MOF precursors (Fig. 4C and D),

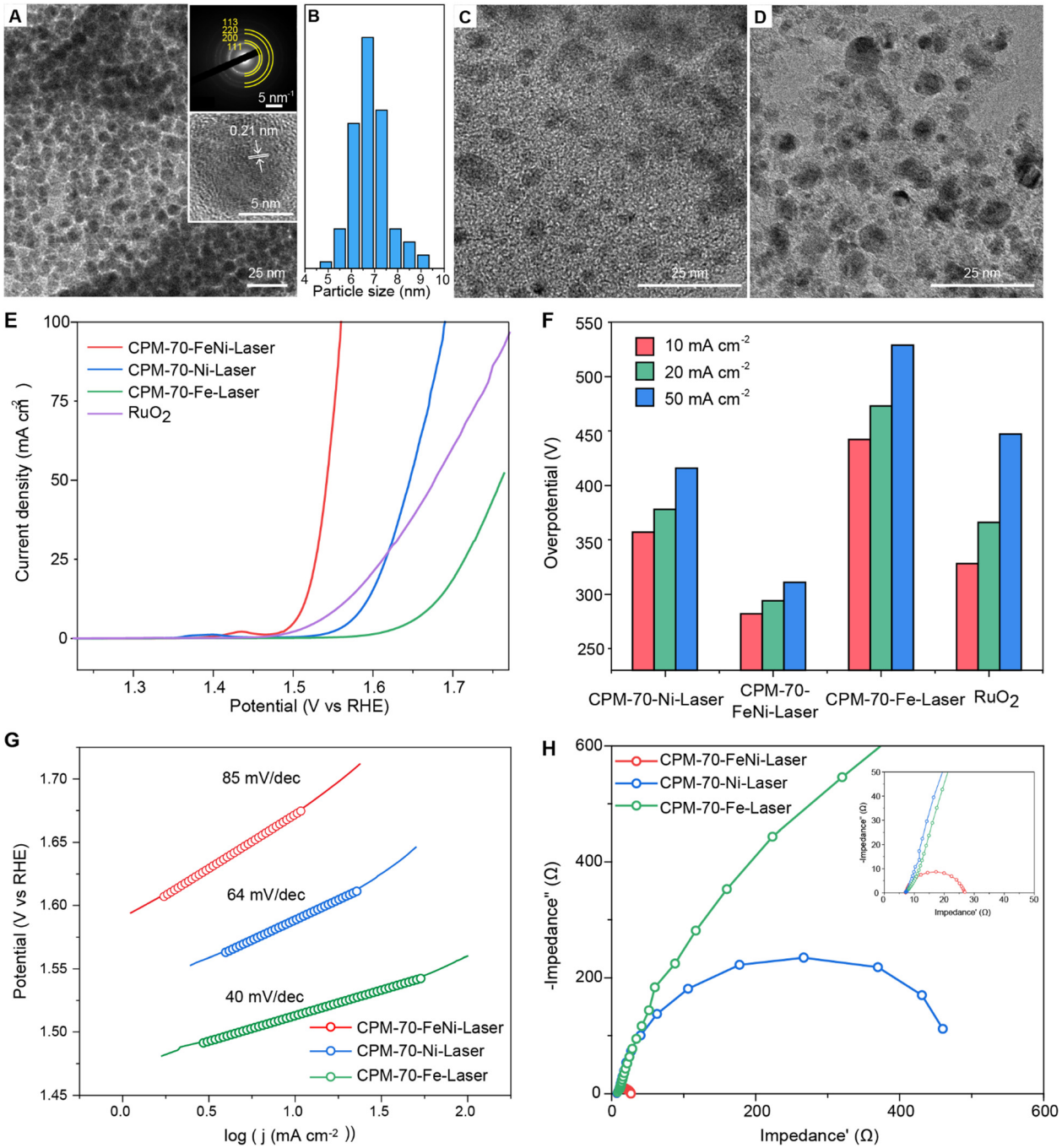


Fig. 4 (A) TEM image and (B) the particle size distribution of the FeNi alloy nanoparticles. TEM images of (C) Fe and (D) Ni nanoparticles from laser conversion of CPM-70-Fe and CPM-70-Ni, respectively. (E) The LSV curves of the metal nanoparticles and nanoalloys from laser metallurgy of the corresponding MOF precursors in the OER reaction. The commercial $RuO_2$ catalyst was also tested as a control under identical conditions. (F) The performance comparison of different catalysts in overpotentials under different currents. (G) The Tafel plots of different metal nanoparticle catalysts. (H) The electrochemical impedance spectroscopy (EIS) of metal nanoparticle catalysts from laser metallurgy of the corresponding MOF precursor.

suggesting that the MTV-MOF strategy can regulate the morphology of the nanoparticles. The chemical state of the elements in the nanoalloys was analyzed by X-ray photoelectron spectroscopy (XPS) (Fig. S53, ESI†). We found that most of the transition metals, Mn, Fe, Co, Ni, Zn, and Cu, were in zero oxidation state with partial oxidation on the surface, consistent with previous reports.[7] The existence of the carbonaceous support was proved by the Raman spectra of the CPM-70-M-laser samples (Fig. S54, ESI†). Two peaks located at Raman shifts of 1050 and 1350 $cm^{-1}$ are ascribed to the D and G band of graphite.[32] The existence of a peak at 2600 $cm^{-1}$ suggested the formation of few-layered graphene in the product, which would benefit the electron transfer in electrochemical reactions.

Nanoalloys are widely used as catalysts in energy and environmental fields.[4–6] The catalytic performance of the uniform FeNi nanoalloys from laser nanometallurgy was demonstrated in the oxygen evolution reaction (OER) for electrochemical water splitting. Linear sweep voltammetry (LSV) curves of laser-induced samples were recorded to evaluate their OER performance (Fig. 4E). The binary CPM-70-FeNi-laser exhibited the lowest potential at a fixed current density of 10 mA $cm^{-2}$, smaller than that of CPM-70-Ni-laser, CPM-70-Fe-laser and the commercial $RuO_2$ catalyst. The overpotentials measured at a current density of 10, 20 and 50 mA $cm^{-2}$ are listed in Fig. 4F. The binary CPM-70-FeNi-laser catalyst delivered the smallest overpotential of 282 mV at a fixed current density of 10 mA $cm^{-2}$, while CPM-70-Ni-laser, CPM-70-Fe-laser and $RuO_2$ catalysts showed higher overpotentials of 357 mV, 442 mV and 328 mV, respectively, under identical conditions. A similar trend was found when the current density increased to 20 and 50 mA $cm^{-2}$ (Fig. 4F). The Tafel curves of the samples were recorded to investigate the reaction kinetics of the catalysts (Fig. 4G). The binary CPM-70-FeNi-laser catalyst showed a smallest slope of 40 mV $dec^{-1}$ among these samples, suggesting its fast oxygen evolution kinetics. Electrochemical impedance spectroscopy (EIS) was further performed at a fixed potential of 1.51 V *vs.* RHE to uncover the charge transfer impedance in the catalysts (Fig. 4H). The binary CPM-70-FeNi-laser catalyst exhibited the smallest charge transfer resistance ($R_{ct}$) in the three catalysts, indicating the excellent electron transfer in the nanoalloy catalysts. The alloying strategy by laser nanometallurgy of MTV-MOF provides rich choices for the fabrication of nanoalloys with excellent catalytic performance.

In summary, the MTV-MOF strategy was successfully applied to incorporate various metal ions in a series of isoreticular MOFs for the synthesis of alloy nanoparticles. The high compatibility of the metal clusters in these MTV-MOFs provides exceptional dispersion of the metal ions in the precursor and the laser metallurgy method benefits the ultrafast reaction kinetics. We believe that this method will shed new light on the fabrication of HEANPs derived from MOFs because of the huge MOF family and their MTV-MOF variants.

## Conflicts of interest

There are no conflicts to declare.

## Acknowledgements

We thank the Core Research Facilities of College of Chemistry and Molecular Sciences for assistance with material characterizations. We acknowledge support from the National Natural Science Foundation of China (22025106 and 21971199), the National Key Research and Development Project (2018YFA 0704000), the Innovation Team of Wuhan University (2042017 kf0232) and the Postdoctoral innovation research positions in Hubei Province.

## References

1 P. C. Chen, X. Liu, J. L. Hedrick, Z. Xie, S. Wang, Q. Y. Lin, M. C. Hersam, V. P. Dravid and C. A. Mirkin, A. Polyelemental nanoparticle libraries, *Science*, 2016, **352**, 1565–1569.
2 C. Xie, Z. Niu, D. Kim, M. Li and P. Yang, Surface and interface control in nanoparticle catalysis, *Chem. Rev.*, 2019, **120**, 1184–1249.
3 H. Duan, D. Wang and Y. Li, Green chemistry for nanoparticle synthesis, *Chem. Soc. Rev.*, 2015, **44**, 5778–5792.
4 X. Huang, Z. Zhao, L. Cao, Y. Chen, E. Zhu, Z. Lin, M. Li, A. Yan, A. Zettl, Y. M. Wang, X. Duan, T. Mueller and Y. Huang, High-performance transition metal-doped $Pt_3Ni$ octahedra for oxygen reduction reaction, *Science*, 2015, **348**, 1230–1234.
5 Q. L. Zhu, J. Li and Q. Xu, Immobilizing metal nanoparticles to metal-organic frameworks with size and location control for optimizing catalytic performance, *J. Am. Chem. Soc.*, 2013, **135**, 10210–10213.
6 W. T. Koo, J. E. Millstone, P. S. Weiss and I. D. Kim, The design and science of polyelemental nanoparticles, *ACS Nano*, 2020, **14**, 6407–6413.
7 Y. Yao, Z. Huang, P. Xie, S. D. Lacey, R. J. Jacob, H. Xie, F. Chen, A. Nie, T. Pu, M. Rehwoldt, D. Yu, M. R. Zachariah, C. Wang, R. S. Yassar, J. Li and L. Hu, Carbothermal shock synthesis of high-entropy-alloy nanoparticles, *Science*, 2018, **359**, 1489–1494.
8 H. Jiang, X. Liu, M. N. Zhu, J. Xu, L. An, P. F. Sui, J. L. Luo and G. J. Cheng, Nanoalloy libraries from laser-induced thermionic emission reduction, *Sci. Adv.*, 2022, **8**, eabm6541.
9 D. Wu, K. Kusada, Y. Nanba, M. Koyama, T. Yamamoto, T. Toriyama, S. Matsumura, O. Seo, I. Gueye, J. Kim, L. S. R. Kumara, O. Sakata, S. Kawaguchi, Y. Kubota and H. Kitagawa, Noble-Metal High-Entropy-Alloy Nanoparticles: Atomic-Level Insight into the Electronic Structure, *J. Am. Chem. Soc.*, 2022, **144**, 3365–3369.
10 L. Tao, M. Sun, Y. Zhou, M. Luo, F. Lv, M. Li, Q. Zhang, L. Gu, B. Huang and S. Guo, A General Synthetic Method for High-Entropy Alloy Subnanometer Ribbons, *J. Am. Chem. Soc.*, 2022, **144**, 10582–10590.
11 S. Gao, S. Hao, Z. Huang, Y. Yuan, S. Han, L. Lei, X. Zhang, R. S.-Yassar and J. Lu, Synthesis of high-entropy alloy nanoparticles on supports by the fast moving bed pyrolysis, *Nat. Commun.*, 2020, **11**, 1–10.
12 N. L. Broge, M. Bondesgaard, F. S. Pedersen, M. Roelsgaard and B. B. Iversen, Autocatalytic Formation of High-Entropy Alloy Nanoparticles, *Angew. Chem., Int. Ed.*, 2020, **132**, 22104–22108.
13 H. Qiao, M. T. Saray, X. Wang, S. Xu, G. Chen, Z. Huang, C. Chen, G. Zhong, Q. Dong, M. Hong, H. Xie, R. S. Yassar and L. Hu, Scalable synthesis of high entropy alloy nanoparticles by microwave heating, *ACS Nano*, 2021, **15**, 14928–14937.
14 E. P. George, D. Raabe and R. O. Ritchie, High-entropy alloys, *Nat. Rev. Mater.*, 2019, **4**, 515–534.
15 G. Pacchioni, High-entropy materials go nano, *Nat. Rev. Mater.*, 2022, **7**, 156.

16 H. C. Zhou, J. R. Long and O. M. Yaghi, Introduction to metal-organic frameworks, *Chem. Rev.*, 2012, **112**, 673–674.
17 H. C. Zhou and S. Kitagawa, Metal–organic frameworks (MOFs), *Chem. Soc. Rev.*, 2014, **43**, 5415–5418.
18 H. Deng, C. J. Doonan, H. Furukawa, R. B. Ferreira, J. Towne, C. B. Knobler, B. Wang and O. M. Yaghi, Multiple functional groups of varying ratios in metal–organic frameworks, *Science*, 2010, **327**, 846–850.
19 L. J. Wang, H. Deng, H. Furukawa, F. Gándara, K. E. Cordova, D. Peri and O. M. Yaghi, Synthesis and Characterization of Metal–Organic Framework-74 Containing 2, 4, 6, 8, and 10 Different Metals, *Inorg. Chem.*, 2014, **53**, 5881–5883.
20 K. A. White, D. A. Chengelis, K. A. Gogick, J. Stehman, N. L. Rosi and S. Petoud, Near-Infrared Luminescent Lanthanide MOF Barcodes, *J. Am. Chem. Soc.*, 2009, **131**, 18069–18071.
21 B. Tu, L. Diestel, Z.-L. Shi, W. R. L. Nisansala Bandara, Y. Chen, W. Lin, Y.-B. Zhang, S. G. Telfer and Q. Li, Harnessing Bottom-Up Self-Assembly To Position Five Distinct Components in an Ordered Porous Framework, *Angew. Chem., Int. Ed.*, 2019, **58**, 5348–5353.
22 C. C. Blas, N. L. Salas, M. C. Gutiérrez, I. P. Orench, E. G. Puebla, M. L. Ferrer, M. Á. Monge and F. Gándara, Encoding Metal–Cation Arrangements in Metal−Organic Frameworks for Programming the Composition of Electrocatalytically Active Multimetal Oxides, *J. Am. Chem. Soc.*, 2019, **141**, 1766–1774.
23 H. F. Wang, L. Chen, H. Pang, S. Kaskel and Q. Xu, MOF-derived electrocatalysts for oxygen reduction, oxygen evolution and hydrogen evolution reactions, *Chem. Soc. Rev.*, 2020, **49**, 1414–1448.
24 H. Jiang, S. Jin, C. Wang, R. Ma, Y. Song, M. Gao, X. T. Liu, A. G. Shen, G. J. Cheng and H. Deng, Nanoscale laser metallurgy and patterning in air using MOFs, *J. Am. Chem. Soc.*, 2019, **141**, 5481–5489.
25 R. Ma, H. Jiang, C. Wang, C. Zhao and H. Deng, Multivariate MOFs for laser writing of alloy nanoparticle patterns, *Chem. Commun.*, 2020, **56**, 2715–2718.
26 W. Zhang, W. Yan, H. Jiang, C. Wang, Y. Zhou, F. Ke, H. Cong and H. Deng, Uniform Bi-Sb alloy nanoparticles synthesized from MOFs by laser metallurgy for sodium-ion batteries, *ACS Sustainable Chem. Eng.*, 2020, **8**, 335–342.
27 Q. Wang and D. Astruc, State of the art and prospects in metal-organic framework (MOF)-based and MOF-derived nanocatalysis, *Chem. Rev.*, 2019, **120**, 1438–1511.
28 X. Zhao, C. Mao, K. T. Luong, Q. Lin, Q. G. Zhai, P. Feng and X. Bu, Framework Cationization by Preemptive Coordination of Open Metal Sites for Anion-Exchange Encapsulation of Nucleotides and Coenzymes, *Angew. Chem., Int. Ed.*, 2016, **55**, 2768–2772.
29 S. Yao, D. Wang, Y. Cao, G. Li, Q. Huo and Y. Liu, Two stable 3D porous metal-organic frameworks with high performance for gas adsorption and separation, *J. Mater. Chem. A*, 2015, **3**, 16627–16632.
30 J. Jia, X. Lin, C. Wilson, A. J. Blake, N. R. Champness, P. Hubberstey, G. Walker, E. J. Cussen and M. Schröder, Twelve-connected porous metal-organic frameworks with high $H_2$ adsorption, *Chem. Commun.*, 2007, 840–842.
31 Y. S. Wei, K. J. Chen, P. Q. Liao, B. Y. Zhu, R. B. Lin, H. L. Zhou, B. Y. Wang, W. Xue, J. P. Zhang and X. M. Chen, Turning on the flexibility of isoreticular porous coordination frameworks for drastically tunable framework breathing and thermal expansion, *Chem. Sci.*, 2013, **4**, 1539–1546.
32 H. Jiang, L. Tong, H. Liu, J. Xu, S. Jin, C. Wang, X. Hu, L. Ye, H. Deng and G. J. Cheng, Graphene-metal-metastructure monolith *via* laser shock-induced thermochemical stitching of MOF crystals, *Matter*, 2020, **2**, 1535–1549.

 